Scripta Materialia 194 (2021) 113691

Contents lists available at ScienceDirect

Scripta Materialia

journal homepage: www.elsevier.com/locate/scriptamat

Atypical transport for $GdTe_{1.8}$ upon substitution with Se: Strong electron-phonon coupling in polaronic conduction

Hagen Poddig[a,b], Dean Hobbis[b], Thomas Doert[a,*], George S. Nolas[b,*]

[a] Faculty of Chemistry and Food Chemistry, Technische Universität Dresden, 01062 Dresden, Germany
[b] Department of Physics, University of South Florida, Tampa, FL, 33620, USA

ARTICLE INFO

Article history:
Received 1 September 2020
Revised 14 December 2020
Accepted 18 December 2020
Available online 5 January 2021

Keywords:
Polaron transport
Rare earth metal
Electrical conductivity
Semiconductors

ABSTRACT

The chemistry of new materials and the effects of chemical substitutions on physical properties continues to be of intense interest as it directly affects many technological fields. The synthesis and temperature dependent transport properties of $GdTe_{1.62}Se_{0.18}$ were investigated revealing polaronic transport upon simple alloying with selenium. Temperature-dependent resistivity and thermopower measurements indicate strong electron-phonon coupling, as compared to the few other chalcogenides that display such transport. In addition, the low thermal conductivity is intrinsic for this material, and a result of the stacking arrangement in the crystal structure as well as of a statistical disordered Te_2^{2-} anion.

Binary lanthanide chalcogenides $REX_{2-\delta}$ (RE = Y, La–Nd, Sm, Gd–Lu; X = S, Se or Te; $0 \leq \delta \leq 0.2$) continue to be intensively investigated because of the quite large structural changes that are realized in only a small compositional range, as well as the physical properties variations that these structural variations induce [1]. The general structure of these materials can be thought of as alternating stacks of a puckered [REX] layer and a planar [X] layer. For the case of the stoichiometric REX_2 compounds, this planar layer is best described as a distorted square net of X_2^{2-} anions. Reducing the chalcogenide content results in vacancies in the planar [X] layer, which are usually compensated by the formation of isolated X^{2-} anions to maintain the overall charge in the layer [1]. Tellurides show significant structural differences to their sulphur and selenium counterparts as they form larger polyanionic fragments such as the XeF_2 analogous Te_3^{4-} anion reported for $RETe_{1.8}$ (RE = Sm, Gd–Dy) [2–4]. The $REX_{2-\delta}$ compounds are generally semiconductors with decreasing band gaps, E_g, in the sequence from tellurides to selenides and sulphides. The reported E_g for the tellurides differs slightly depending on composition, with values of 0.14 eV for $NdTe_{1.89(1)}$ [5], 0.19 eV for $GdTe_{1.8}$ [2] and 0.04 for $SmTe_{1.84}$ [6]. We note that $LaTe_2$ is an exception to this list as metallic behaviour has been reported for this compound [7].

In addition to the interest in the structural chemistry of these $RETe_{1.8}$ materials, the physical properties thus far reported concentrated mainly on the magnetic and electrical properties. The thermal transport is much less investigated. A recent report on the transport properties and how chemical substitution affects the electrical and thermal properties in $GdTe_{1.8}$ revealed a low thermal conductivity that is presumably typical for these materials [8]. Herein we report on the effects of Se-substitution for Te in $GdTe_{1.8}$. Isovalent Se was chosen for its comparable chemical behavior to Te, i.e. no direct hole or electron doping, in order to investigate the temperature dependent thermal and electrical properties upon such substitution.

All preparatory steps for the synthesis were carried out in a nitrogen filled glovebox. In a standard synthesis, 3 g of a stoichiometric mixture of Gd_2Te_3, Te (Alfa Aesar, 99.999 %) and Se (Alfa Aesar, 99.9%) were placed in a quartz tube and sealed under dynamic vacuum ($p \leq 1 \times 10^{-3}$ mbar). A small amount of iodine (~0.02 equivalents to $GdTe_{1.8}$) was added to the reaction mixture to enhance the mass transport and to ensure a complete reaction. The reaction mixture was heated to 1073 K and held at this temperature for 5 days. The prepared specimens were stored and handled in a nitrogen atmosphere. The precursor Gd_2Te_3 was prepared analogously by reacting elemental Gd (99.5%, MaTecK) and Te (Merck, > 99.9%, reduced in H_2 stream at 400°C) in a glassy carbon crucible inside a fused silica ampoule. The fine ground powder was heated to 1073 K and held at this temperature for 4 days. The ampoule was opened in the glovebox and the purity of the precursor was checked by powder X-ray diffraction.

Powder X-ray diffraction (PXRD) data of the synthesized, powdered specimens were collected on a Bruker D8 focus diffractometer in Bragg-Brentano geometry with CuKα radiation and a graphite receiving monochromator. Rietveld refinement was per-

* Coressponding authors.
E-mail addresses: thomas.doert@tu-dresden.de (T. Doert), gnolas@usf.edu (G.S. Nolas).

https://doi.org/10.1016/j.scriptamat.2020.113691
1359-6462/

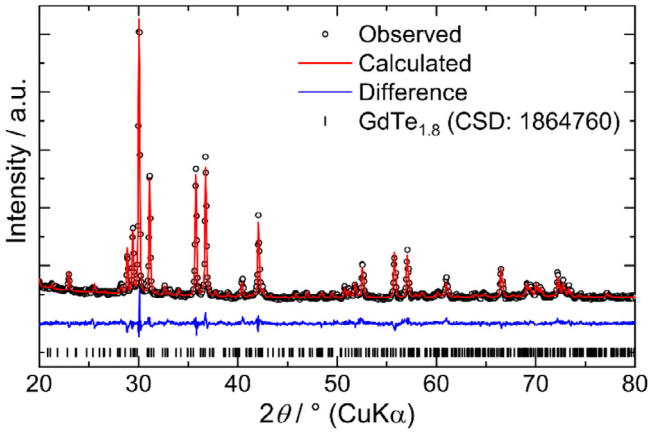

Fig. 1. Rietveld-refinement of the powder x-ray diffraction pattern of $GdTe_{1.62}Se_{0.18}$. As a starting model the crystal structure of $GdTe_{1.8}$ has been used. Upon substitution no peak splitting or additional reflections were observed.

formed with TOPAS, using the fundamental parameter approach [9].

The specimens were ground into fine powder, sieved (325 mesh) and placed inside a custom-designed WC die and punch assembly that was lined with graphite foil to prevent reactions with the surrounding material for densification. Densification was performed by spark plasma sintering (SPS) under vacuum at 523 K and 400 MPa for 30 minutes. The maximum temperature for densification was evaluated by differential thermal analysis and thermal gravimetric analysis using a TA Instruments Q600 to ensure that the specimens did not undergo oxidation or degradation during the densification process.

Temperature dependent transport measurements were performed on 2 × 2 × 5 mm^3 parallelepipeds that were cut using an abrasive slurry wire saw. Temperature dependent four-probe resistivity (ρ), Seebeck coefficient (S) and steady-state thermal conductivity (κ) measurements were performed on a custom-built radiation-shielded vacuum probe [10,11]. The electrical contacts were made by directly soldering to Ni plated surfaces and Stycast epoxy was used for the thermal contacts. The maximum experimental uncertainties for these measurements are 7% for ρ, 6% for S and 8% for κ measurements.

Le Bail profile fitting and Rietveld refinement of the powder XRD pattern utilizing the basic $GdTe_{1.8}$ structure indicated a small shrinkage of the lattice parameters compared to $GdTe_{1.8}$ (Fig. 1). As substitution for these structures are less investigated, previous reports on substituting parts of the chalcogen by an pnictogen [12–15] or by a different chalcogen [16,17] indicate a general trend. The most electronegative and electropositive element will occupy the puckered [*REX*] double layer, whereas the medium electronegative element occupies the planar [*X*] layer [18] (see Fig. 2). This suggests a substitution of Se on the Te site in the puckered [GdTe] layer due to its higher electronegativity (2.55 vs. 2.1) [19]. Several reports support this hypothesis, as seen for the series $LaS_{2-x}Se_x$ ($0 \leq x \leq 2$) [16] and $GdSb_xTe_{2-x-\delta}$ [20]. In the $RESeTe_2$ compound (RE = La–Nd, Sm), which crystallizes in the directly related $NdTe_3$ structure, Se is exclusively observed in the puckered double layer [*REX*] [21], hinting towards a similar situation for mixed selenium and tellurium compounds of a hypothetical $RETe_{2-x}Se_x$ series.

The temperature-dependent ρ data is shown in Fig. 3, with the inset displaying the temperature-dependent S data. As in the case of $GdTe_{1.8}$, ρ increases with decreasing temperature for $GdTe_{1.62}Se_{0.18}$ at higher temperatures, which is characteristic of semiconductor behaviour. The E_g value can be estimated from the high temperature ρ data employing a fit of the form $\rho = \rho_0 exp(E_g/2k_BT)$ where k_B is the Boltzmann constant and T is the absolute temperature. The measured band gap of 0.23 eV is similar to that reported for $GdTe_{1.8}$ (0.19 eV) [2]. In addition, the ρ data displays a temperature dependence that is different from that of typical semiconducting behaviour, with an anomalous peak in the ρ vs. T data at 39 K. A structural transformation cannot explain this dramatic change in the ρ and S data at low temperatures, and no evidence of a low-temperature structural transformation have been observed for this structure type [2,8]. The localized peak observed differs from the typical behaviour seen in other binary tellurides, such as MnTe [22] and Bi_2Te_3 [23], however, a similar behaviour has been observed in pentatellurides, such as $HfTe_5$ and $ZrTe_5$, where the peak in the low temperature ρ data was attributed to polaronic conduction [24]. More evidence to suggest polaronic conduction can be seen from the S data, as shown in the inset of Fig. 3, which shows a large peak occurring at the same temperature as that for the ρ data. These data indicate po-

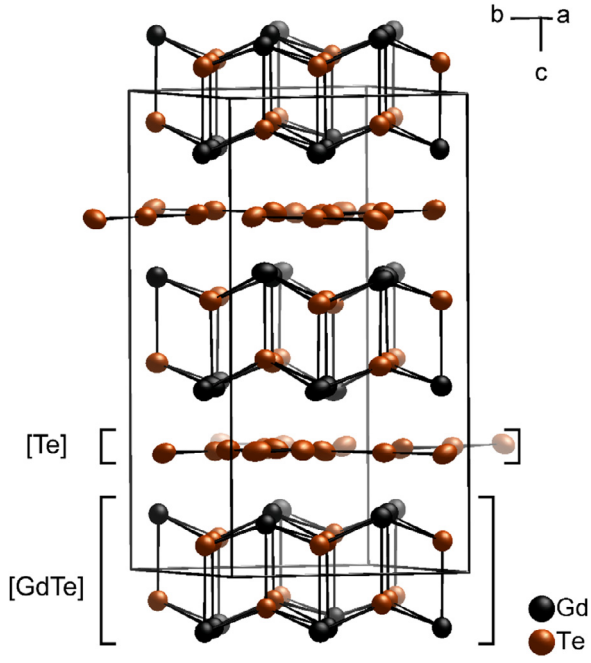

Fig. 2. Crystal structure of $GdTe_{1.8}$. The two different layers of the general motif are highlighted.

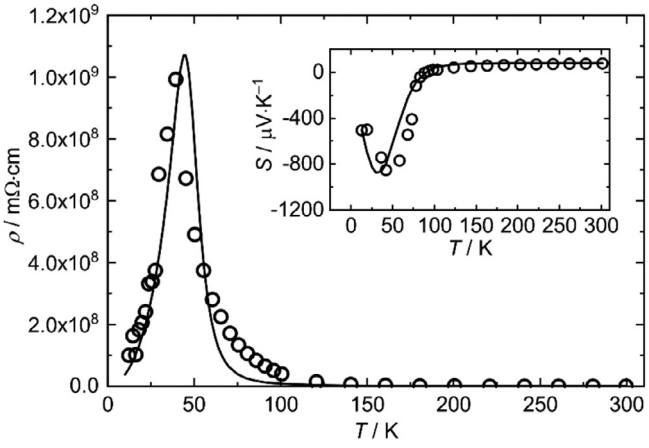

Fig. 3. Temperature-dependent ρ for $GdTe_{1.62}Se_{0.18}$, where the solid line fit is from the dual component Holstein model. The inset shows temperature-dependent S data along with a fit to this model. The fit is over the entire measured temperature range.

Table 1
Fit parameters from the two-component model.

	B_i	A_h	E_a/k_B (K)	T_0 (K)	Δ (K)
$GdTe_{1.62}Se_{0.18}$	295000	260	543	39	23

laron transport [25]. The nature of this phenomena was originally described by Holstein [25], owing the behaviour to carrier-phonon coupling that results in self-trapping of the carriers, defined as polarons. This behaviour gives rise to a maximum in ρ at lower temperatures due to competing mechanisms. In the low temperature regime, the trapped carriers can form a conducting band with heavy mass that corresponds to an itinerant polaron band. The higher temperature regime is characterized by thermally activated induced polaron hopping, where the polarons become localized because of inelastic absorption and emission of phonons that begin to dominate [24,25]. The peak can be modelled using the competing mechanisms, from the itinerant polaron band and polaron "hopping", by employing

$$\rho(T) = \left[\frac{f(T)}{\rho_i(T)} + \frac{1-f(T)}{\rho_h(T)}\right]^{-1}, \quad (1)$$

where

$$f\ (T) = \frac{1}{2}\left[1 - \tanh\left(\frac{T-T_0}{\Delta}\right)\right][24]. \quad (2)$$

Here $\rho_i(T)$ is the itinerant mechanism, $\rho_h(T)$ is the thermally activated hopping, T_0 is the temperature corresponding to the maximum ρ and Δ is a constant associated with the transition width determined from the experimental data. The itinerant and thermally activated hopping can be described by,

$$\rho_i(T) = B_i T^2, \quad (3)$$

and

$$\rho_h(T) = A_h T e^{(E_a/k_B T)}, \quad (4)$$

where B_i and A_h are constants to be determined from the experimental fitting, E_a is the thermal activation energy and k_B is the Boltzmann constant. The values of this fit are shown in Table 1. The fit parameters B_i and A_h are much larger than those reported for $ZrTe_5$, which shows much smaller peak ρ values, while they are similar to those reported for $Ag_2ZnSnSe_4$, a material that shows comparable ρ values and polaron transport [24,26,27]. The parameter E_a is related to the upturn and sharpness in ρ(T) in the intermediate range. The resistive peak occurs for our specimen at 39 K, a lower temperature than for $ZrTe_5$ and $Ag_2ZnSnSe_4$, which may indicate stronger carrier-phonon coupling at lower temperature for $GdTe_{1.62}Se_{0.18}$. Furthermore, the Debye temperature, ϑ_D, can be estimated using $T_0 \cong \vartheta_D$ / 2 [24,25], resulting in ϑ_D = 78 K for $GdTe_{1.62}Se_{0.18}$. The Δ value is similar to that reported for $ZrTe_5$ and describes the width of the peak and thus the transition to the quantum-mechanical transitions at low temperatures.

The inset of Fig. 3 shows the S vs. T data, with a large negative peak in S at the same temperature as that for ρ. At temperatures below this transition, S tends to zero, as would be expected, while above the transition S becomes smaller in magnitude before turning positive and relatively constant as charge carriers are no longer trapped at higher temperatures. A fit to the S data of the form,

$$S(T) = [f(T)][D_S][-cT] + [1-f(T)][S_H] \quad (5)$$

is also shown in Fig. 3, where D_S, c and S_H are constants determined from the fit. The value of c that we obtain is 0.85, which relates to the number of polarons per available site. This value is larger than that reported for $HfTe_5$ and suggests a larger effective polaron concentration [24], which is consistent with the larger magnitude of the S and ρ peaks observed here for $GdTe_{1.62}Se_{0.18}$.

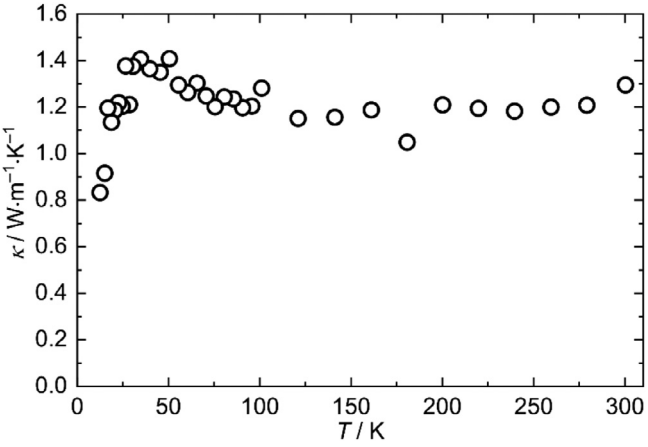

Fig. 4. Temperature-dependent κ for $GdTe_{1.62}Se_{0.18}$.

The κ values measured for $GdTe_{1.62}Se_{0.18}$ (Fig. 4) are relatively low and comparable to chalcogenides such as Bi_2Te_3 alloys as well as other low κ materials that are of interest for potential applications where low κ values are required, in thermoelectrics for example [23,28–32]. The low κ values are apparently intrinsic to these materials and may be attributed, in part, to the complex crystal structure and a statistical disorder of a Te_2^{2-} fragment in the anionic [Te] layer.

To conclude, we synthesized polycrystalline $GdTe_{1.62}Se_{0.18}$ and investigated its structure and temperature dependent transport properties for the first time. The low temperature S and ρ data reveal atypical transport, which can be attributed to polaronic conduction, as analysed using the dual component Holstein model. This analysis indicates a significant electron-phonon coupling upon substitution with Se in $GdTe_{1.8}$. In addition, the κ values are low and intrinsic to this material. This work reveals how elemental substitution can strongly impact transport in layered chalcogenides, and significantly enhances our understanding of the structure-property relationships in layered binary lanthanide chalcogenide materials.

This work was support by the US National Science Foundation under grant No. DMR-1748188. HP gratefully acknowledges the support of the ERASMUS+ ICM WORLDWIDE exchange program funded by the European Union. Financial Support by the German Research Foundation (DFG, grant no. Do 590/6-1) is also gratefully acknowledged. DH acknowledges the II-VI Foundation Block-Gift Program.

Declaration of Competing Interest

The authors declare that they have no known competing financial interests or personal relationships that could have appeared to influence the work reported in this paper.

References

[1] T. Doert, C.J. Müller, Reference Module in Chemistry, Molecular Sciences and Chemical Engineering, Elsevier, 2016.
[2] H. Poddig, T. Donath, P. Gebauer, K. Finzel, M. Kohout, Y. Wu, P. Schmidt, T. Doert, Z. Anorg. Allg. Chem. 644 (2018) 1886–1896.
[3] I. Ijjaali, J.A. Ibers, J. Solid State Chem. 179 (2006) 3456–3460.
[4] L.D. Gulay, J. Stępień-Damm, M. Daszkiewicz, A. Pietraszko, J. Alloys Compd. 427 (2007) 166–170.
[5] K. Stöwe, Z. Kristallogr. - Cryst. Mater. 216 (2001) 215–224.
[6] S.-M. Park, S.-J. Park, S.-J. Kim, J. Solid State Chem. 140 (1998) 300–306.
[7] K. Stöwe, J. Solid State Chem. 149 (2000) 155–166.
[8] H. Poddig, D. Hobbis, N. Alzahrani, T. Doert, G.S. Nolas, Eur. J. Inorg. Chem. 2020 (2020) 2424–2427.
[9] A.A. Coelho, J. Appl. Crystallogr. 51 (2018) 210–218.
[10] J. Martin, S. Erickson, G.S. Nolas, P. Alboni, T.M. Tritt, J. Yang, J. Appl. Phys. 99 (2006) 044903.

[11] J. Martin, G.S. Nolas, Rev. Sci. Instrum. 87 (2016) 015105.
[12] L. Hoistad Strauss, C.M. Delp, J. Alloys Compd. 353 (2003) 143–145.
[13] R. Niewa, A. Czulucki, M. Schmidt, G. Auffermann, T. Cichorek, M. Meven, B. Pedersen, F. Steglich, R. Kniep, J. Solid State Chem. 183 (2010) 1309–1313.
[14] A. Schlechte, R. Niewa, H. Borrmann, G. Auffermann, M. Schmidt, R. Kniep, Z. Kristallogr. - New Cryst. Struct. 222 (2014) 369–370.
[15] M. Schmidt, T. Cichorek, R. Niewa, A. Schlechte, Y. Prots, F. Steglich, R. Kniep, J. Phys.: Condens. Matter 17 (2005) 5481–5488.
[16] C. Bartsch, T. Doert, J. Solid State Chem. 185 (2012) 101–106.
[17] C. Bartsch, T. Doert, Solid State Sci 14 (2012) 515–521.
[18] P. Böttcher, T. Doert, H. Arnold, R. Tamazyan, Z. Kristallogr. - Cryst. Mater. 215 (2000) 246–253.
[19] L. Pauling, The Nature of the Chemical Bond, Cornell University Press, Ithaca, New York, 1960 Third Edition.
[20] S. Lei, V. Duppel, J.M. Lippmann, J. Nuss, B.V. Lotsch, L.M. Schoop, Adv. Quantum Technol. 2 (2019) 1900045.
[21] B.P. Fokwa Tsinde, T. Doert, Solid State Sci 7 (2005) 573–587.
[22] J.D. Wasscher, Electrical Transport Phenomena in MnTe, an Antiferromagnetic Semiconductor, Technische Hogeschool Eindhoven, 1969 Phd Thesis.
[23] G.S. Nolas, J. Sharp, J. Goldsmid, Thermoelectrics: Basic Principles and New Materials, 1st ed., Springer-Verlag, Berlin, Heidelberg, 2001.
[24] M. Rubinstein, Phys. Rev. B 60 (1999) 1627–1632.
[25] T. Holstein, Ann. Phys. 281 (2000) 706–724.
[26] K. Wei, A.R. Khabibullin, T. Stedman, L.M. Woods, G.S. Nolas, J. Appl. Phys. 122 (2017) 105109.
[27] K. Wei, G.S. Nolas, ACS Appl. Mater. Interfaces 7 (2015) 9752–9757.
[28] S.J. Gomez, D. Cheikh, T. Vo, P. Von Allmen, K. Lee, M. Wood, G.J. Snyder, B.S. Dunn, J.-P. Fleurial, S.K. Bux, Chem. Mater. 31 (2019) 4460–4468.
[29] F. Pabst, D. Hobbis, N. Alzahrani, H. Wang, I.P. Rusinov, E.V. Chulkov, J. Martin, M. Ruck, G.S. Nolas, J. Appl. Phys. 126 (2019) 105105.
[30] G.A. Lamberton, R.H. Tedstrom, T.M. Tritt, G.S. Nolas, J. Appl. Phys. 97 (2005) 113715.
[31] G.S. Nolas, G.A. Slack, Am. Sci. 89 (2001) 136–141.
[32] Y. Dong, H. Wang, G.S. Nolas, Phys. Status Solidi RRL 8 (2014) 61–64.